ANL-6778 ANL-6778

Argonne National Laboratory

STRUCTURAL ANALYSIS OF FARET CORE SUPPORTS UNDER MECHANICAL AND THERMAL LOADINGS

by

M. M. Chen

LEGAL NOTICE

This report was prepared as an account of Government sponsored work. Neither the United States, nor the Commission, nor any person acting on behalf of the Commission:

A. Makes any warranty or representation, expressed or implied, with respect to the accuracy, completeness, or usefulness of the information contained in this report, or that the use of any information, apparatus, method, or process disclosed in this report may not infringe privately owned rights; or

B. Assumes any liabilities with respect to the use of, or for damages resulting from the use of any information, apparatus, method, or process disclosed in this report.

As used in the above, "person acting on behalf of the Commission" includes any employee or contractor of the Commission, or employee of such contractor, to the extent that such employee or contractor of the Commission, or employee of such contractor prepares, disseminates, or provides access to, any information pursuant to his employment or contract with the Commission, or his employment with such contractor.

Printed in USA. Price $2.00. Available from the Clearinghouse for Federal
Scientific and Technical Information, National Bureau of Standards,
U. S. Department of Commerce, Springfield, Virginia

ANL-6778
Engineering and Equipment
(TID-4500, 37th Ed.)
AEC Research and
Development Report

ARGONNE NATIONAL LABORATORY
9700 South Cass Avenue
Argonne, Illinois 60440

STRUCTURAL ANALYSIS OF FARET CORE SUPPORTS UNDER MECHANICAL AND THERMAL LOADINGS

by

M. M. Chen

Reactor Engineering Division

Prepared September 1963
Published September 1964

Operated by The University of Chicago
under
Contract W-31-109-eng-38
with the
U. S. Atomic Energy Commission

TABLE OF CONTENTS

Page

ABSTRACT 7

I. INTRODUCTION 7

II. ANALYSIS 13

III. APPLICATION TO FARET REACTOR GRID PLATES 19

- A. Core Model and Loading Conditions 19
- B. Deformation of Grid Plates 20
- C. Stress Components 24
  - 1. Bending Stresses 24
  - 2. Membrane Stress Components 27
- D. Ligament Efficiency 28
- E. Limit Stresses for Design of Perforated Plates 28

IV. CONCLUDING REMARKS 31

ACKNOWLEDGMENTS 31

REFERENCES 32

LIST OF FIGURES

No. Title Page

1. Core Section 8
2. Core Support Grid and Cylinder 9
3. Notations for a Perforated Plate 9
4. Reactor Vessel 10
5. Grid-structure Supporting Arrangements 11
6. Coordinate Systems for a Circular Plate 14
7. Variation of ∆T for Various Values of n 15
8. Coordinate System and Mechanical Loads for Model of FARET Grid Plates 19
9. Temperature Distributions for FARET Model 20
10. Deflection Distributions for Top Plate 21
11. Deflection Distributions for Top Plate 21
12. Deflection Distributions for Top Plate, Combined Pressure and Temperature Effects 22
13. Maximum Deflection vs. Plate Thickness 23
14. Maximum Deflection vs. Plate Thickness 23
15. Maximum Deflection vs. Plate Thickness, Combined Pressure and Temperature Effects 23
16. Radial Stress Distributions, Top Plate 25
17. Circumferential Stress Distributions, Top Plate. 25
18. Stress at Center vs. Plate Thickness 26
19. Radial Stress at Edge vs. Plate Thickness. 26
20. Circumferential Stress at Edge vs. Plate Thickness 26
21. Effective Elastic Constants for Perforated Plates. 28

LIST OF TABLES

No.	Title	Page
1.	Core Geometries	8
2.	Preliminary Design Requirements of FARET Reactor	11
3.	Loading Conditions for FARET Model	19
4.	Maximum Deflections for Grid Plates	24
5.	Radial Stress Distribution for a Typical Loading Condition (k = 0)	27
6.	Circumferential Stress Distribution for a Typical Loading Condition (k = 0)	27
7.	Ligament Stress Intensity σ_{eff} and Peak Stress Intensity σ_{max} for FARET Model (k = 0)	30

STRUCTURAL ANALYSIS OF FARET CORE SUPPORTS UNDER MECHANICAL AND THERMAL LOADINGS

by

M. M. Chen

ABSTRACT

A structural analysis was made (Sept 1963) of the core support grid of the Fast Reactor Test Facility (FARET). This structure consists of three circular plates which form high- and low-pressure plenums for achieving a coolant flow distribution. These plates are perforated for insertion of the fuel rods. The weight of the fuel assemblies and the coolant pressures in the plenums constitute the principal mechanical loading of the core support grid. In addition, thermal loadings arise because of the temperature distributions in the grid.

A general solution has been developed for the stress analysis of a core support plate which is subjected to these mechanical and thermal loadings for any rotationally restrained edge conditions. The resulting deflections and stresses were computed for various loading conditions by use of the IBM-704 computer. For the thermal analysis, a rotationally symmetric temperature distribution was assumed, varying linearly through the thickness of the plate. The analysis was based on classical small-deflection theory and the concept of the "equivalent solid plate" of O'Donnell and Langer. The solution was applied to a model which simulates the FARET core support subjected to a combined mechanical and thermal loading.

I. INTRODUCTION

The Fast Reactor Test (FARET) program is an experimental program directed toward the demonstration of breeder reactors which are essential to the long-range goal of utilizing fertile fuels.(1) The facility is planned and designed for carrying out experimental work involving both reactor engineering performance, and reactor dynamics and safety. The areas of investigation in engineering performance will be those involving fuel and fuel-clad concepts and designs, high power densities and high temperatures, high fissile atom burnup, and system operating experience expected in an actual power breeder. The dynamics and safety investigations will include the determination of nuclear characteristics in connection with the stability and safety of large dilute systems, and the observation of reactivity effects due to the change in temperature of fuel, sodium, and clad. The temperature changes will simulate the actual operating conditions of a fast breeder. Detailed descriptions of some well-planned experiments are given in Ref. 1.

Because of the particular objectives of the experimental programs, three separate cores are needed for the FARET reactor, namely, (1) a zoned core, (2) a medium core, and (3) a small core. The basic plan of the reactor core is shown in Fig. 1, and the possible core sizes, excluding the reflectors, are shown in Table 1. Inside each core three types of subassemblies (fuel, control and reflector) comprise the static loading, each of which conforms to a common design subassembly. Each subassembly is hexagonal in shape; the outer dimension is 2.29 in. across flats (see Fig. 2). The weight of each subassembly is 150 lb, and the total static load of a full complement of subassemblies is about 90,000 lb. All the subassemblies are maintained in a lattice spacing of 2.32 in. (see Fig. 3). The holes are distributed symmetrically with respect to the center of the plate and are arranged in an equilateral pattern.

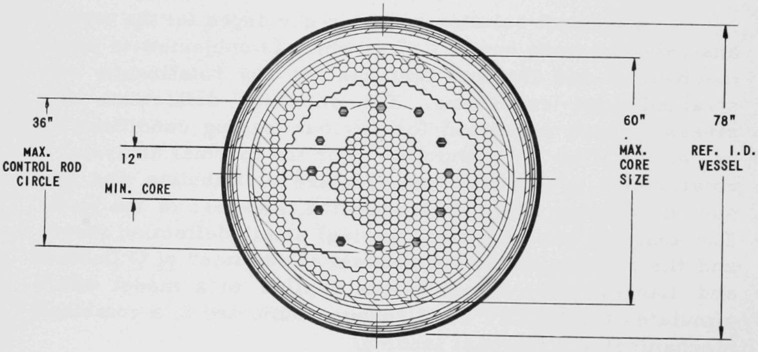

Fig. 1 Core Section

Table 1

CORE GEOMETRIES
(Approximate)

Core Parameter	Small Core	Medium Core	Zoned Core
Volume (liters)	40	400	1400
Diameter (cm)	44	95	150
Length (cm)	33	70	120

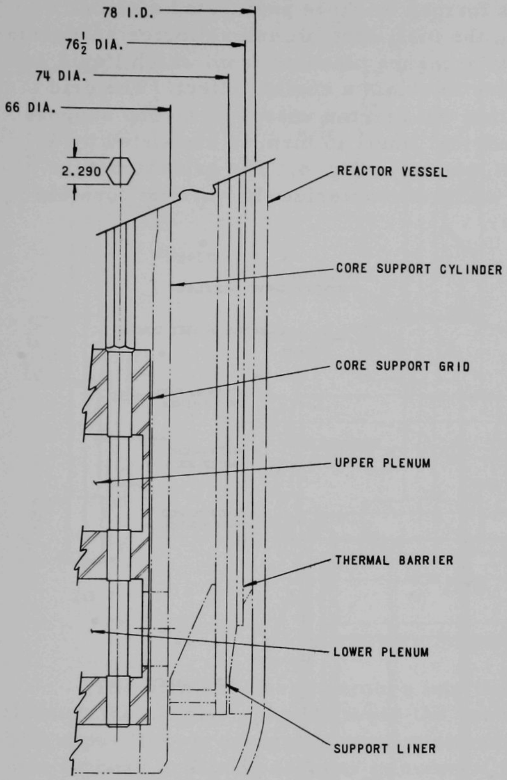
78 I.D.
76½ DIA.
74 DIA.
66 DIA.
2.290
REACTOR VESSEL
CORE SUPPORT CYLINDER
CORE SUPPORT GRID
UPPER PLENUM
THERMAL BARRIER
LOWER PLENUM
SUPPORT LINER

Fig. 2

Core Support Grid and Cylinder

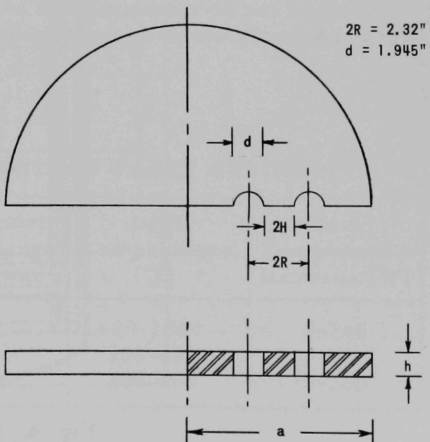
2R = 2.32"
d = 1.945"
d
2H
2R
h
a

Fig. 3

Notations for a Perforated Plate

The core support grid is formed by three perforated circular plates. In addition to supporting the fuel, control, and reflector subassemblies, it forms the high- and low-pressure plenums from which liquid sodium flows into the subassemblies to obtain a cooling effect. The grid structure itself is supported within the reactor vessel by a core support cylinder (see Fig. 2). The cylindrical liner, in turn, is supported by a flange at the reactor vessel wall, shown in Fig. 4. The grid-structure models chosen for the analysis which characterize the various possible designs are shown in Fig. 5.

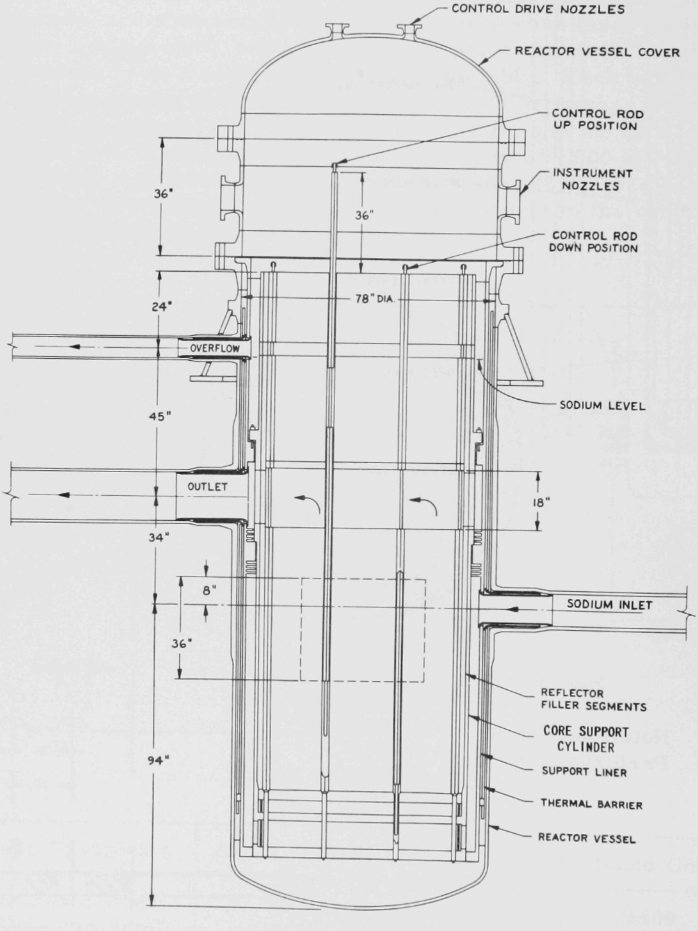
CONTROL DRIVE NOZZLES
REACTOR VESSEL COVER
CONTROL ROD UP POSITION
INSTRUMENT NOZZLES
CONTROL ROD DOWN POSITION
36"
36"
24"
78" DIA.
OVERFLOW
SODIUM LEVEL
45"
OUTLET
18"
34"
8"
SODIUM INLET
36"
REFLECTOR FILLER SEGMENTS
CORE SUPPORT CYLINDER
SUPPORT LINER
94"
THERMAL BARRIER
REACTOR VESSEL

Fig. 4. Reactor Vessel

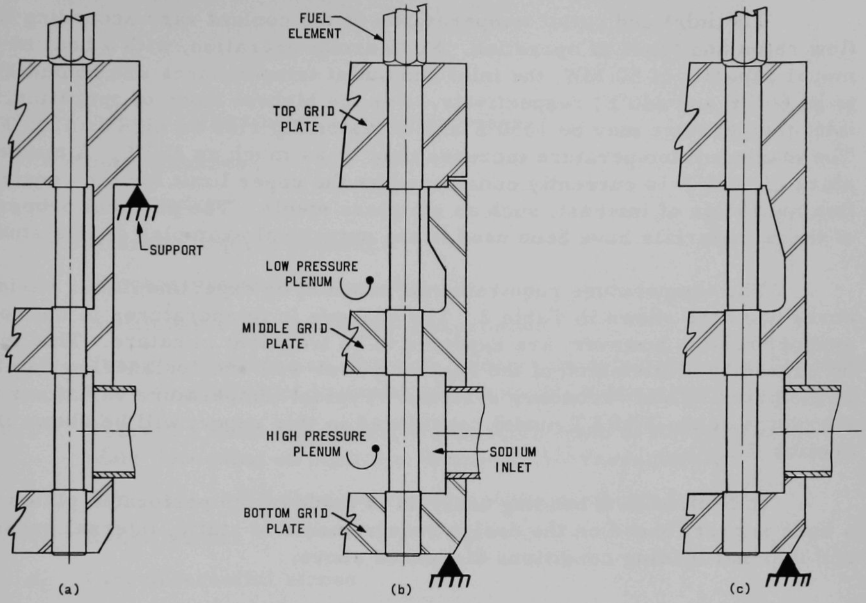
FUEL ELEMENT
TOP GRID PLATE
SUPPORT
LOW PRESSURE PLENUM
MIDDLE GRID PLATE
HIGH PRESSURE PLENUM
SODIUM INLET
BOTTOM GRID PLATE
(a)
(b)
(c)

Fig. 5. Grid-structure Supporting Arrangements

The primary coolant enters into the lower (high-pressure) plenum through the annular space between the vessel and the core support cylinder. The upper (low-pressure) plenum receives the coolant from the lower plenum through orificed passages in some of the outer subassembly adaptors. The inlet pressures caused by the pumps may vary from a few psi to 85 psi in the lower plenum, and from a few psi to approximately 45 psi in the upper plenum. The maximum design pressure imposed by the planned experiments is 85 psi (see Table 2).

Table 2

PRELIMINARY DESIGN REQUIREMENTS OF FARET REACTOR$^{(2)}$

Core	Flow Rate (gpm @1000°F)	Inlet and Outlet Pressure Change (psi @6000 gpm)	Inlet Temperature (°F)	Core Temperature Increase (°F)
Small	600-6000	85	600-1000	0-240
Medium	600-6000	85	300-400	0-100
Zoned	600-6000	85	300-400	0-100

The inlet and outlet temperatures of the coolant vary according to flow rates and types of operation. For normal operation, with a heat removal capacity of 50 MW, the inlet and outlet temperatures are considered to be 600°F and 840°F, respectively. For the highest mode of operation, the inlet temperature may be 1050°F and occasionally rise as high as 1200°F. The maximum temperature increase may be as much as 300°F. A temperature of 1200°F is currently considered as the upper limit for the construction materials of interest, such as stainless steels. The physical properties of these materials have been used in the numerical examples of this study.

The temperature requirements imposed by experiments for various cores are also shown in Table 2. The changes in temperatures in the core support region, however, are expected to be transient in nature. This may be caused by a mismatch of the reactor power with the coolant flow rates in the primary and secondary systems. Typical temperature variations for the plates of the FARET model considered in this report will be shown in Section III.

In Section II, a bending analysis is made of the perforated plates of a core support based on the design requirements of static, internal pressure, and thermal loading conditions discussed above.

II. ANALYSIS

Nomenclature

W	lateral deflection of plate midsurface
h	plate thickness
a	plate radius
p	laterally applied pressure
T	temperature distribution, Eq. (3)
α	coefficient of linear thermal expansion
E, E^*	Young's modulus and effective Young's modulus of the perforated plate depending on ligament efficiency,(3) respectively
ν, ν^*	Poisson's ratio and effective Poisson's ratio of the perforated plate depending on ligament efficiency,(3) respectively
D^*	$E^*h^3/12[1 - \nu^{*2}]$, flexural rigidity of the perforated plate(3)
σ_r	Radial stress
σ_θ	Circumferential stress
σ'_r	Radial membrane stress
σ'_θ	Circumferential membrane stress
M_r	Radial bending moment per unit circumferential length
M_θ	Circumferential bending moment per unit circumferential length
M_t	Thermal moment per unit circumferential length
k	Rotational restraint factor
A_n, B_n	Temperature constants (where $n = 0, 1$, etc.)
∇^2	$\frac{d^2}{dr^2} + \frac{1}{r}\frac{d}{dr}$, Laplacian operator
r, z	radial and axial coordinates, respectively

The calculation of stresses and deflections of a reactor core support system is one of the major undertakings during the preliminary stage of a reactor design. The three perforated plates of the core support structure considered in this report will be designated as the top, middle, and bottom grid plates (see Fig. 6). The perforations of these plates are in an equilateral triangular pattern so that the "equivalent plate theory" of O'Donnell and Langer(3) is applicable.

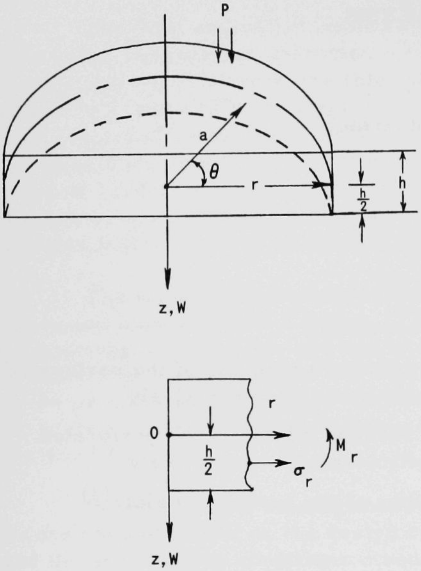

Fig. 6

Coordinate Systems
for a Circular Plate

The static load due to the various subassemblies is applied only to the top plate, whereas internal pressures and thermal gradients are exerted on all three plates. The boundary conditions are such that the deflections must vanish and that the angles of rotation may vary on the boundary in an arbitrary manner. In the following, a bending analysis for a perforated circular plate under prescribed loads is developed. The classical linear theory is used.

The governing differential equation(4) for the bending of circular plates made of an isotropic material of uniform thickness subjected to a temperature gradient and a lateral pressure is extended to the perforated case as follows:

$$D^* \nabla^2 \nabla^2 W = p - \frac{1}{1 - \nu^*} \nabla^2 M_t \qquad (1)$$

where

$$M_t = \alpha E^* \int_{-h/2}^{h/2} Tz \, dz. \qquad (2)$$

The coordinate system used is shown in Fig. 6.

The temperature is assumed to vary linearly through the thickness of the plate and to be axially symmetric. It is assumed that the temperature distribution can be expressed by a convergent power series:

$$T(r,z) = T_0(r) - \frac{z}{h} \sum_{n=0}^{\infty} A_n r^n, \qquad (3)$$

where the A_n's are constant and $A_n r^n$ has the same dimension as temperature. The radial temperature distribution at the midsurface of the plate is given by $T_0(r)$. It is seen from Eq. (3) that the temperature decreases as z increases if the A_n have positive values. The terms containing $A_n r^n$ represent the temperature difference between the upper and lower faces for various values of r (Fig. 7). It is to be noted from Eq. (2) that the thermal moment vanishes when temperature variations with z are symmetrical with respect to the midsurface of the plate. The solution for membrane stresses due to thermal forces has been found previously.(4,5) The determination of the combined bending and membrane stresses for the core support model will be given in Section III.

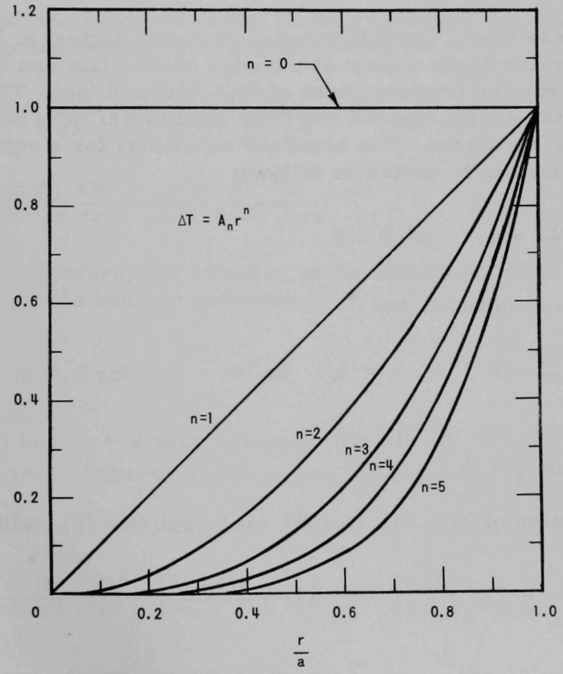

Fig. 7. Variation of ΔT for Various Values of n

The mathematical boundary conditions for a simply supported or a clamped plate are generally expressed by the following equations:

$$\frac{dW(0)}{dr} = 0; \qquad W(a) = 0; \qquad M_r(a) = 0 \tag{4a, 4b, 4c}$$

for simply supported plates, and

$$\frac{dW(0)}{dr} = 0; \qquad W(a) = 0; \qquad \frac{dW(a)}{dr} = 0 \tag{5a, 5b, 5c}$$

for clamped plates. However, neither of the limiting conditions, Eq. (4c) or Eq. (5c), is encountered in practice. For example, the clamped condition at the edge is rarely realized because no practical mounting can be built for a plate support with infinite rigidity. The question as to whether the plate is simply supported or clamped depends upon the relative stiffness of the plate and its support, and the means of joining. The exact degree of restraint requires experimental verification.

In this report an edge rotation restraint factor, k, is introduced such that the angular displacement at the edge of the plate can be taken to be anywhere between the limiting cases of Eqs. (4c) and (5c). This restraint factor along with the energy method has been used in Ref. 6 to analyze the EBR-II reactor grid structure. The boundary conditions for a rotationally restrained plate can be stated as follows:

$$\frac{dW(0)}{dr} = 0; \qquad W(a) = 0 \tag{4a, 4b}$$

for all edge conditions, and

$$\frac{dW(a)}{dr} = 0 \quad \text{for } k = 1; \qquad M_r(a) = 0 \quad \text{for } k = 0, \tag{6}$$

where $0 \leq k \leq 1$. For the simply supported case $k = 0$, and for the fully restrained edge $k = 1$.

Solution of Eqs. (1), (2), (3), (4a), (4b), and (6) yields

$$\frac{W}{h} = \frac{3}{16}\frac{p}{E^*}\left(\frac{a}{h}\right)^4 (1 - \nu^{*2})\left\{\left[1 + \frac{4(1-k)}{1+\nu^*}\right] - 2\left[1 + \frac{2(1-k)}{1+\nu^*}\right]\left(\frac{r}{a}\right)^2 + \left(\frac{r}{a}\right)^4\right\}$$

$$+ \frac{(1+\nu^*)\alpha}{2}\left(\frac{a}{h}\right)^2 \sum_{n=0}^{\infty} \frac{A_n a^n}{(n+2)^2}\left\{\left[n - \frac{2(n+2)(1-k)}{1+\nu^*}\right]\right.$$

$$\left. - (n+2)\left[1 - \frac{2(1-k)}{1+\nu^*}\right]\left(\frac{r}{a}\right)^2 + 2\left(\frac{r}{a}\right)^{n+2}\right\}, \tag{7}$$

provided the pressure is uniform. For a nonuniform lateral pressure, $p = p(r)$, a particular solution, W_p, may be obtained through the successive integration:

$$W_p(r) = \int^{r} \frac{1}{r_4} \int^{r_4} r_3 \int^{r_3} \frac{1}{r_2} \int^{r_2} \frac{r_1\, p(r_1)}{D^*}\, dr_1 dr_2 dr_3 dr_4. \tag{8}$$

The arbitrary constants for the general solution must be determined from the boundary conditions, Eqs. (4a), (4b), and (6).

If there is no thermal gradient, the solution of Eq. (7) for $k = 0$, and $k = 1$, reduces the deflections due to the mechanical load obtained in Ref. 7. Similarly, for the thermal gradient only, and for $k = 0$ and $k = 1$, Eq. (7) reduces to the solution obtained in Ref. 8.

The radial and circumferential bending moments are related to the lateral deflection and thermal moment as follows:(4)

$$M_r = -D^*\left(\frac{d^2W}{dr^2} + \frac{\nu^*}{r}\frac{dW}{dr}\right) - \frac{M_t}{1-\nu^*}; \tag{9}$$

$$M_\theta = -D^*\left(\frac{1}{r}\frac{dW}{dr} + \nu^*\frac{d^2W}{dr^2}\right) - \frac{M_t}{1-\nu^*}. \tag{10}$$

The radial and circumferential stresses at the upper and lower faces of the plate are related to the bending moments:(4)

$$\sigma_r = 6M_r/h^2; \tag{11}$$

$$\sigma_\theta = 6M_\theta/h^2. \tag{12}$$

The sign conventions of these quantities are indicated in Fig. 6.

Substitution of Eq. (7) into Eqs. (9) and (10) yields, respectively,

$$\overline{M}_r = \frac{1}{16}\left(\frac{p}{E^*}\right)\left(\frac{a}{h}\right)^2\left[(3+\nu^*-2k) - (3+\nu^*)\left(\frac{r}{a}\right)^2\right]$$

$$- \frac{\alpha}{12(1-\nu^*)}\sum_{n=0}^{\infty}\frac{A_n a^n}{(n+2)}\left[(1-\nu^*-2k) - (1-\nu^*)\left(\frac{r}{a}\right)^n\right]; \tag{13}$$

$$\overline{M}_\theta = \frac{1}{16}\left(\frac{p}{E^*}\right)\left(\frac{a}{h}\right)^2\left[(3+\nu^*-2k) - (1+3\nu^*)\left(\frac{r}{a}\right)^2\right]$$

$$- \frac{\alpha}{12(1-\nu^*)}\sum_{n=0}^{\infty}\frac{A_n a^n}{(n+2)}\left[(1-\nu^*-2k) - (n+1)(1-\nu^*)\left(\frac{r}{a}\right)^n\right], \qquad (14)$$

where $\overline{M}_r$ and $\overline{M}_\theta$ are nondimensional quantities:

$$\overline{M}_r = M_r/(E^*h^2); \qquad \overline{M}_\theta = M_\theta/(E^*h^2).$$

The temperature variation ΔT is defined as $A_n r^n$, and its graphical representation for $n = 0$ to $n = 5$ is shown in Fig. 7. The bending stresses can be obtained from Eqs. (11) to (14) for a given ΔT. The application of the solution obtained to the preliminary design of the FARET reactor grid plates is shown in the next section.

III. APPLICATION TO FARET REACTOR GRID PLATES

A. Core Model and Loading Conditions

A typical model of the FARET grid plates is shown in Fig. 8. The mid-surface is taken at $z = 0$ for each plate, and the same symbols as used in Section II are used for all three plates. The loading conditions due to the static load, internal pressure, and temperature variations are shown in Table 3

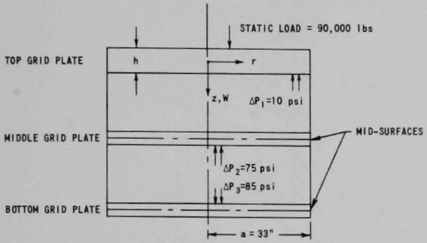
STATIC LOAD = 90,000 lbs
TOP GRID PLATE
h
r
z, W
ΔP1=10 psi
MIDDLE GRID PLATE
MID-SURFACES
ΔP2=75 psi
ΔP3=85 psi
BOTTOM GRID PLATE
a = 33"

Fig. 8

Coordinate System and Mechanical Loads for Model of FARET Grid Plates

Table 3

LOADING CONDITIONS FOR FARET MODEL

(See Figs. 8 and 9)

Loads / Plates	Static Load (lb)	Δp (psi)	Temperature Distribution** (°F)			
			B_0	B_1a	A_0	A_1a
Top	90 000*	-10	0	37.5	0	-25
Middle	0	-75	25	30	-50	10
Bottom	0	85	25	10	-50	0

* The static load is assumed to be uniformly distributed over the entire plate.

** The temperature distribution is expressible as follows:

$$T(r,z) = B_0 + B_1 r - \frac{z}{h}(A_0 + A_1 r) \tag{15}$$

and in Figs. 8 and 9. It is seen from Table 3 that when $n = 0$ and $n = 1$, the term $T_0(r)$ in Eq. (3) takes the following form:

$$T_0(r) = B_0 + B_1 r, \tag{16}$$

where B_0 and B_1 are constants, and $B_1 r$ has the same dimension as temperature. The above postulated temperature distribtuions in the grid plates are based on the assumption that the coolant temperature at the inlet to the structure changes occasionally as much as 50°F during a fraction of a minute. Such a change in temperature might be caused by a mismatch of the reactor power with the coolant flow rates in the primary and/or secondary systems.

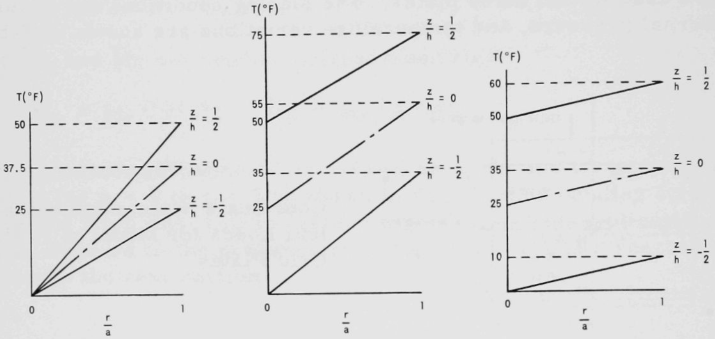

(a) TOP GRID PLATE

(b) MIDDLE GRID PLATE

(c) BOTTOM GRID PLATE

Fig. 9. Temperature Distributions for FARET Model

Assuming this rapid 50°F change, it was estimated that the thermal response of the grid plates would be slow enough to produce the z-direction temperature gradients used. The temperature gradient in the r-direction is based on the effects of coolant-transport time as well as energy losses from the coolant as it passes the structure, which is at a lower temperature. These temperature considerations are based on the small-zone core configurations; on the other hand, the static load is calculated for a full complement of 595 fuel elements acting on the top plate of the zone core. This corresponds to the highest thermal and static stresses, respectively.

B. Deformation of Grid Plates

It is seen from Eq. (7) that the lateral deflection due to a uniform temperature distribution across the plate, i.e., n = 0, and linear temperature distribtuion, i.e., n = 1, is determined by

$$\begin{aligned}\frac{W}{h} = {} & \frac{3}{16}\frac{p}{E^*}\left(\frac{a}{h}\right)^4(1-\nu^{*2})\left\{\left[1+\frac{4(1-k)}{1+\nu^*}\right]-2\left[1+\frac{2(1-k)}{1+\nu^*}\right]\left(\frac{r}{a}\right)^2+\left(\frac{r}{a}\right)^4\right\} \\ & -\frac{\alpha}{2}\left(\frac{a}{h}\right)^2 A_0(1-k)\left[1-\left(\frac{r}{a}\right)^2\right] \\ & +\frac{(1+\nu^*)\alpha}{18}\left(\frac{a}{h}\right)^2 A_1 a\left\{\left[1-\frac{6(1-k)}{1+\nu^*}\right]-\left[3-\frac{6(1-k)}{1+\nu^*}\right]\left(\frac{r}{a}\right)^2+2\left(\frac{r}{a}\right)^3\right\}. \qquad (17)\end{aligned}$$

The maximum deflection occurs at the center (r = 0) of the plate. The distribution of deflections due to the loadings as described in Table 3, for k = 0, 0.25, 0.5, 0.75, and 1.0, are plotted in Figs. 10 to 12 for the top plate only. It is to be noted that the lateral deflection of the bottom plate is caused by the internal pressure and A_0 only, since $A_1 = 0$ (See Table 3). This deflection can be obtained through interpolation by using the numerical results for the middle plate.

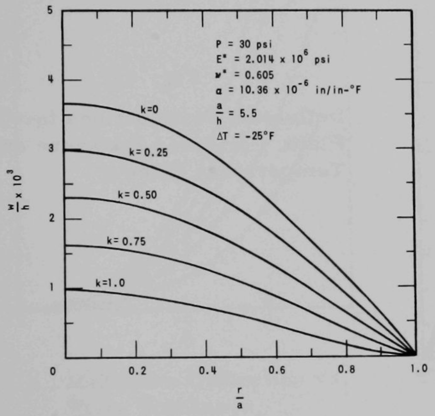

Fig. 10

Deflection Distributions for Top Plate, P = 30 psi

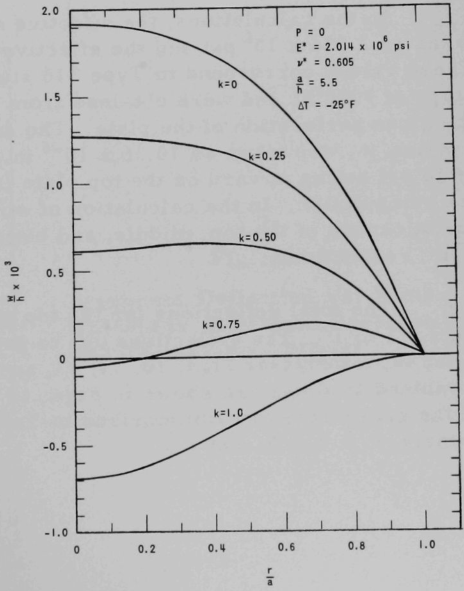

Fig. 11

Deflection Distributions for Top Plate, ΔT = -25°F

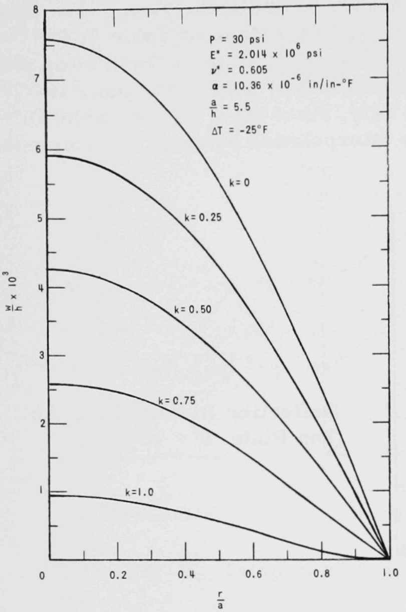

Fig. 12

Deflection Distributions for Top Plate, Combined Pressure and Temperature Effects

In the calculations, the effective modulus of elasticity, E*, was taken as 2.014×10^6 psi and the effective Poisson's ratio, ν^*, as 0.605. These values correspond to Type 316 stainless steel at a service temperature of 1000°F, and were obtained from Fig. 21 (in Section C, below) for the given perforation of the plate. The coefficient of linear thermal expansion, α, was taken as 10.36×10^{-6} in./(in.)(°F). The internal pressure of 10 psi acting upward on the top plate (See Table 3) was not included in the computation. In the calculation of stress and displacement distributions, the thickness of the top, middle, and bottom plates were taken as 6, 4, and 4 in., respectively.

The total deflections for the top plate, including A_0, are plotted in Figs. 13 to 15. The deflections due to pressure and temperature were computed separately (see Figs. 10, 11, 13, and 14). The deflections due to the combined loadings are shown in Figs. 12 and 15. The maximum deflections of the grid plates are summarized in Table 4 for three types of support, namely, k = 0, 0.5, and 1.0.

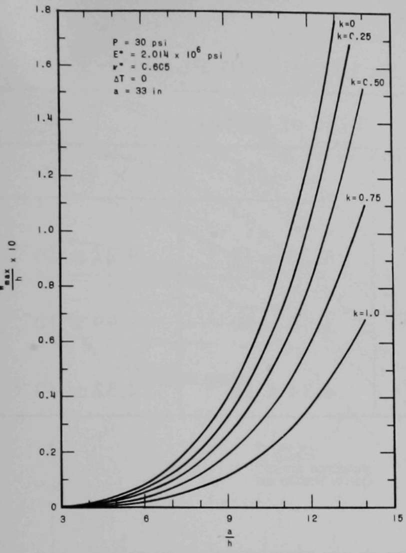

Fig. 13. Maximum Deflection vs. Plate Thickness, P = 30 psi

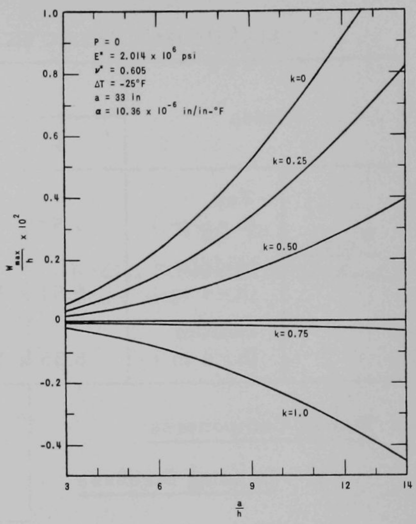

Fig. 14. Maximum Deflection vs. Plate Thickness, ΔT = -25°F

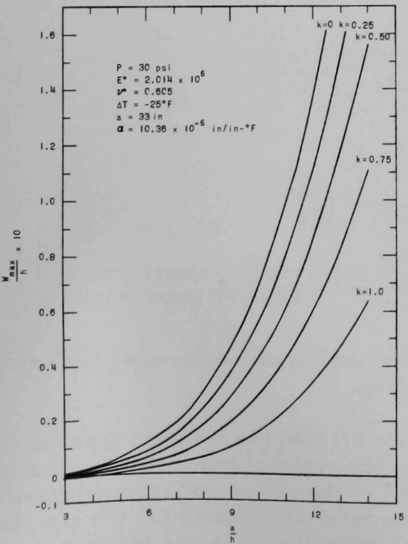

Fig. 15

Maximum Deflection vs. Plate Thickness, Combined Pressure and Temperature Effects

Table 4

MAXIMUM DEFLECTIONS (in.) FOR GRID PLATES

Plates		Type of Support		
		$k = 0$	$k = 0.5$	$k = 1.0$
$\frac{W_{max}}{h}$	Top ($h = 6$ in.)	7.57×10^{-3}	4.25×10^{-3}	9.22×10^{-4}
	Middle ($h = 4$ in.)	-5.57×10^{-2}	-3.78×10^{-2}	-1.99×10^{-2}
	Bottom ($h = 4$ in.)	6.35×10^{-2}	4.34×10^{-2}	2.32×10^{-2}

C. Stress Components

1. Bending Stresses

The radial and circumferential stress components can be found by substituting Eq. (15) into Eqs. (13) and (14) and then into Eqs. (11) and (12):

$$\overline{\sigma}_r = \frac{3}{8}\frac{p}{E^*}\left(\frac{a}{h}\right)^2\left[(3 + \nu^* - 2k) - (3 + \nu^*)\left(\frac{r}{a}\right)^2\right]$$

$$+ \frac{A_0 \alpha k}{2(1 - \nu^*)} + \frac{\alpha A_1 a}{6}\left[\frac{(-1 + \nu^* + 2k)}{(1 - \nu^*)} + \left(\frac{r}{a}\right)\right] \tag{18}$$

and

$$\overline{\sigma}_\theta = \frac{3}{8}\frac{p}{E^*}\frac{a^2}{h}(3 + \nu^* - 2k) - (1 + 3\nu^*)\left(\frac{r}{a}\right)^2$$

$$+ \frac{A_0 \alpha k}{2(1 - \nu^*)} + \frac{\alpha A_1 a}{6}\left[\frac{(-1 + \nu^* + 2k)}{(1 - \nu^*)} + 2\frac{r}{a}\right], \tag{19}$$

where $\overline{\sigma}_r = \sigma_r/E^*$ and $\overline{\sigma}_\theta = \sigma_\theta/E^*$ are nondimensional radial and circumferential stress components due to bending.

It is seen from Eqs. (18) and (19) that the constant thermal-stress term $A_0 \alpha k/[2(1 - \nu^*)]$ depends on the uniform temperature A_0 only. In Figs. 16 and 17, the total distributions of the radial and circumferential stress components including the constant term are plotted for the top plate. In Figs. 18 to 20, the stresses at the center of the plate and the radial circumferential stresses at the plate edge are plotted versus plate thickness for $p = 30$ psi and $\Delta T = -25°F$.

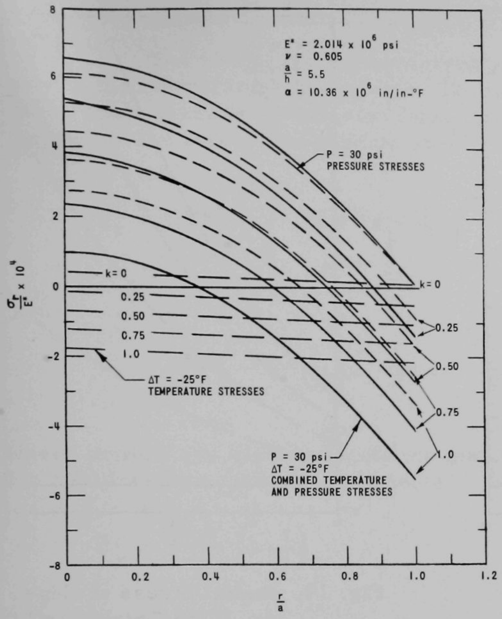

Fig. 16

Radial Stress Distributions, Top Plate

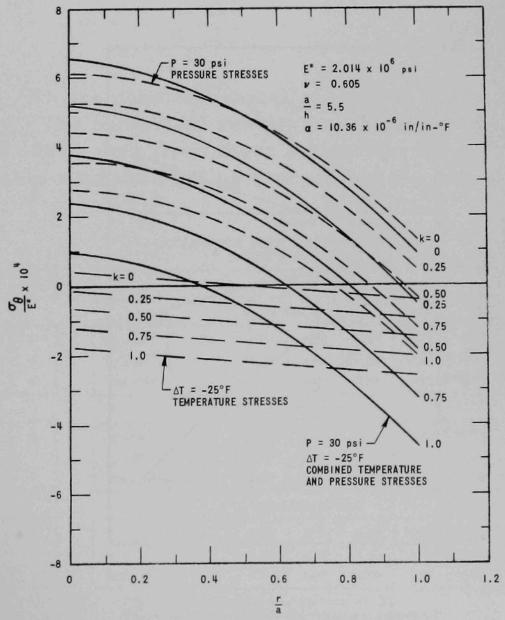

Fig. 17

Circumferential Stress Distributions, Top Plate

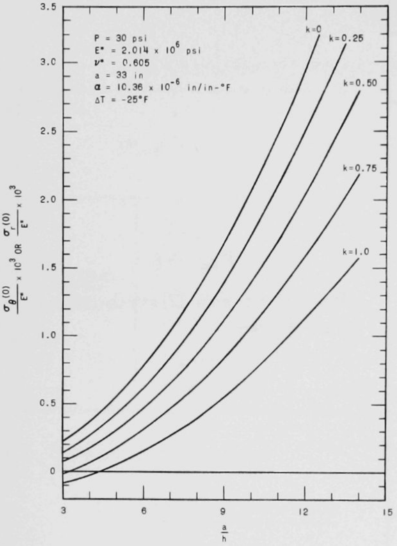

Fig. 18. Stress at Center vs. Plate Thickness

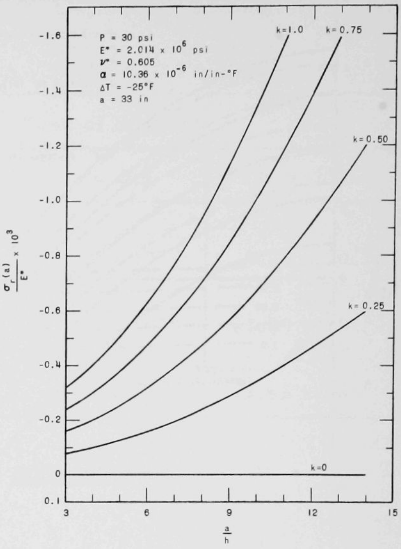

Fig. 19. Radial Stress at Edge vs. Plate Thickness

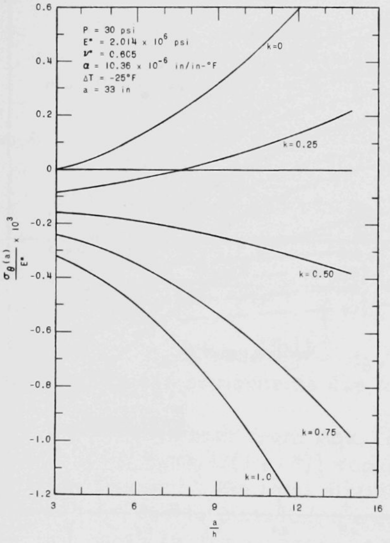

Fig. 20

Circumferential Stress at Edge vs. Plate Thickness

2. Membrane Stress Components

The radial and circumferential membrane stresses are due only to the temperature distribution $T_0(r)$, or B_0 and B_1r, for the present case. Since there is no external force applied to the plane at the boundary, the membrane stress components are$^{(4)}$

$$\sigma'_r = \alpha E^*\left(\frac{1}{a^2}\int_0^a T_0 r\,dr - \frac{1}{r^2}\int_0^r T_0 r\,dr\right) \tag{20}$$

and

$$\sigma'_\theta = \alpha E^*\left(-\,T_0 + \frac{1}{a^2}\int_0^a T_0 r\,dr + \frac{1}{r^2}\int_0^r T_0 r\,dr\right), \tag{21}$$

where primes are used to denote the membrane stress. Substitution of Eq. (16) into Eqs. (20) and (21) yields

$$\bar{\sigma}'_r = \frac{\alpha B_1 a}{3}\left(1 - \frac{r}{a}\right) \tag{22}$$

and

$$\bar{\sigma}'_\theta = \frac{\alpha B_1 a}{3}\left[1 - 2\left(\frac{r}{a}\right)\right], \tag{23}$$

where $\bar{\sigma}'_r = \sigma'_r/E^*$ and $\bar{\sigma}'_\theta = \sigma'_\theta/E^*$ are nondimensional radial and circumferential membrane stresses. The numerical results for typical loadings are shown in Tables 5 and 6. It is seen from these tables that the membrane stresses are comparable with the bending stresses in the top

Table 5

RADIAL STRESS DISTRIBUTION FOR A TYPICAL LOADING CONDITION (k = 0)

	r/a = 0	0.2	0.4	0.6	0.8	1.0
A. Top Plate (h = 6 in.)						
$\bar{\sigma}'_r \times 10^4$*	1.295	1.036	0.777	0.518	0.259	0
$\bar{\sigma}_r \times 10^4$**	6.523	6.193	5.376	4.071	2.279	0
Sum $\times 10^4$	7.818	7.229	6.153	4.589	2.538	0
B. Middle Plate (h = 4 in.)						
$\bar{\sigma}'_r \times 10^4$*	1.036	0.829	0.622	0.414	0.207	0
$\bar{\sigma}_r \times 10^3$**	-3.444	-3.303	-2.889	-2.200	-1.237	0
Sum $\times 10^3$	-3.340	-3.220	-2.827	-2.159	-1.216	0
C. Bottom Plate (h = 4 in.)						
$\bar{\sigma}'_r \times 10^4$*	0.345	0.276	0.207	0.318	0.691	0
$\bar{\sigma}_r \times 10^3$**	3.883	3.728	3.262	2.485	1.398	0
Sum $\times 10^3$	3.918	3.756	3.283	2.517	1.467	0

* $\bar{\sigma}'_r$ denotes radial membrane stress, Eq. (22).

** $\bar{\sigma}_r$ denotes radial bending stress due to pressure and temperature constants, A_0 and A_1, Eq. (18).

Table 6

CIRCUMFERENTIAL STRESS DISTRIBUTION FOR A TYPICAL LOADING CONDITION (k = 0)

	r/a = 0	0.2	0.4	0.6	0.8	1.0
A. Top Plate (h = 6 in.)						
$\bar{\sigma}'_\theta \times 10^4$*	1.295	0.777	0.259	-0.259	-0.777	-1.295
$\bar{\sigma}_\theta \times 10^4$**	6.523	6.160	5.417	4.293	2.788	0.903
Sum $\times 10^4$	7.818	6.937	5.676	4.034	2.011	-0.392
B. Middle Plate (h = 4 in.)						
$\bar{\sigma}'_\theta \times 10^4$*	1.036	0.622	0.207	-0.207	-0.622	-1.036
$\bar{\sigma}_\theta \times 10^3$**	-3.444	-3.330	-3.002	-2.460	-1.704	-0.734
Sum $\times 10^3$	-3.340	-3.268	-2.981	-2.481	-1.766	-0.838
C. Bottom Plate (h = 4 in.)						
$\bar{\sigma}'_\theta \times 10^4$*	0.345	0.207	0.691	-0.691	-0.207	-0.345
$\bar{\sigma}_\theta \times 10^3$**	3.883	3.762	3.398	2.792	1.943	0.851
Sum $\times 10^3$	3.918	3.783	3.467	2.723	1.922	0.816

* $\bar{\sigma}'_\theta$ denotes circumferential membrane stress, Eq. (23).

** $\bar{\sigma}_\theta$ denotes circumferential bending stress due to pressure and temperature constants, A_0 and A_1, Eq. (19).

plate, which is thicker than the others, and that the membrane stresses in remaining plates can be neglected. The underlined quantities are the maximum stresses for each plate.

D. Ligament Efficiency

The method of calculating stresses and deflections in a perforated plate with a triangular penetration pattern has been given by O'Donnell and Langer.(3) They reduced the perforated plate to an "equivalent solid plate" problem by reassigning values to the elastic constants. The effective elastic constants E* and ν^* of the "equivalent solid plate" having the same dimentions of the perforated plate are obtained in Fig. 21. The quantities E* and ν^* depend on the ligament efficiency (ligament efficiency = H/R, see Figs. 3 and 21), and their variations versus ligament efficiency for $H/R > 4$ is shown in Fig. 21. If E* and ν^* are known, the numerical bending and membrane stresses and deflections of an equivalent plate can be calculated from the equations derived in the previous sections. Deflections of the perforated plates are the same as the deflections of the equivalent solid plates. In the FARET core currently considered, 2R = 2.32 in. and 2H = 0.375 in. (see Fig. 3). The ligament efficiency is found to be 0.162.

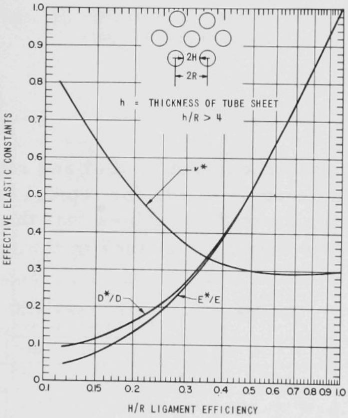

Fig. 21

Effective Elastic Constants for Perforated Plates

E. Limit Stresses for Design of Perforated Plates

In order to design a perforated plate under combined mechanical and thermal loadings, it is proposed in Ref. 3 that ligament stress intensity and peak stress intensity should be the limiting stresses. The ligament stress intensity σ_{eff}, whose calculation is based on the maximum-shear theory of failure, is the average stress across the minimum ligament section, but not through the thickness of the plate. The peak stress intensity $\sigma_{\max}$ is the maximum local stress due to mechanical and thermal loads. However, the peak stress intensity, being localized, is not considered to be the most significant. It is of interest only when it is repeated often enough to produce fatigure. Reference 3 states that for a perforated plate under combined mechanical and thermal loadings:

1. The ligament stress intensity σ_{eff} should be limited to 3 S_m, where S_m is the allowable stress which, according to the 1959 ASME Boiler Code, should not exceed 5/8 of the yield strength of a ferrous material.

2. The peak stress intensities σ_{max} due to any loading should be limited by the cumulative fatigue damage, as described in Refs. 9, 10, and 11.

In the following a sample calculation of the ligament stress intensity σ_{eff} and peak stress σ_{max} is given for the top plate. From Table 5, it is seen that the maximum stress occurs at the center of the plate, and that both the radial and circumferential stresses are the same, i.e., $\bar{\sigma}_r = \bar{\sigma}_\theta = 7.8 \times 10^{-4}$. The quantity $\bar{\sigma}_1$, by definition, equals the larger of $|\bar{\sigma}_r|$ and $|\bar{\sigma}_\theta|$ (see Ref. 3).

Therefore,

$$\bar{\sigma}_1 = 7.8 \times 10^{-4}.$$

Since

$$E^* = 2.014 \times 10^6 \text{ psi},$$

$$\sigma_1 = 1574 \text{ psi},$$

it is found from Fig. 10 of Ref. 3 for

$$\bar{\sigma}_r / \bar{\sigma}_\theta = 1,$$

that the stress intensity factor K = 1. Therefore, the ligament stress intensity can be found as follows (see Ref. 3):

$$\sigma_{eff} = K\left(\frac{R}{H}\right) \sigma_1 = \frac{2.32}{0.375} \times 1574 = 9738 \text{ psi}.$$

Peak stress is defined in Ref. 3 as

$$\sigma_{max} = Y\sigma_1 + p,$$

where p is the pressure acting on the surface and Y the stress ratio, depending upon the ligament efficiency and the state of stresses.

The value Y = 7.6 is obtained from Fig. 12 of Ref. 3 for a ligament efficiency of 0.162. Therefore,

$$\sigma_{max} = 7.6 \times 1574 + 30 = 11992 \text{ psi}.$$

The stress intensities are calculated similarly for the middle and bottom plates. Results are shown in Table 7. For the same ligament efficiency, and depending on the allowable stresses S_m, it is seen that the thickness of the top plate could be reduced and the thicknesses of the remaining plates could be increased. Such an adjustment of the plate thickness would improve the design. Calculations based on the methods of this report would then have to be repeated with the new plate dimensions.

Table 7

LIGAMENT STRESS INTENSITY
σ_{eff} AND PEAK STRESS
INTENSITY σ_{max} FOR FARET
MODEL ($k = 0$)

(psi)

Stress Intensities Plates	σ_{eff}	σ_{max}
Top	9700	12000
Middle	41600	51100
Bottom	48800	60000

IV. CONCLUDING REMARKS

A general solution for the bending of a core support plate subjected to mechanical and thermal loadings was obtained. The solution incorporates boundary conditions having varying degrees of rotational constraint. However, to evaluate the effectiveness of the constraint provided by the supporting structure, one must resort to experimental techniques for establishing the rotational effectiveness. The optimum values of k, the rotational restraint factor, can be obtained by invoking the theorem of minimum total potential energy.

Although the report considers only linear temperature variation through the thickness of the plate, other variations can be readily treated through Eq. (2). The solution obtained was applied to the FARET core support model.

The method of solution can be extended to ring plates, stepped plates, and plates with variable thickness subjected to mechanical and thermal loadings.

ACKNOWLEDGMENTS

The author is indebted to A. Smaardyk for his continuous interest and untiring guidance throughout the investigation. Acknowledgment should be made also to T. R. Bump, W. J. Kann, S. H. Fistedis, and A. Marchertas for their invaluable suggestions and helpful discussions. Special thanks are due to Drs. Fistedis and Marchertas for critically reviewing the final draft.

The numerical results were obtained with the IBM-704 at Argonne. Gratitudes are owed to Mrs. D. Bingaman and her computing group who helped with the computation, and to Miss J. Wilson of the design and drafting group who prepared the figures.

REFERENCES

1. A. Smaardyk et al., Interim Report - FARET Experimental Program, ANL-6708 (April 1963).

2. T. R. Bump, Argonne National Laboratory (Private communication).

3. J. W. O'Donnell and B. F. Langer, Design of Perforated Plates, Trans. ASME, Series B, J. Eng. for Industry 84, 307-320 (Aug 1962).

4. B. A. Boley and J. H. Weiner, Theory of Thermal Stresses, John Wiley & Sons, Inc., New York (1960), pp. 379-405.

5. C. T. Wang, Applied Elasticity, (McGraw-Hill Book Co., Inc., New York (1953), pp. 70-75.

6. A. Marchertas, S. H. Fistedis, and R. O. Brittan, Analysis for Deformation of Nuclear Reactor Grid Structure, ANL-6781 (to be published).

7. S. Timoshenko, Theory of Plates and Shells, (McGraw-Hill Book Co., New York (1940), First Edition, pp. 55-63.

8. M. Forray and M. Newman, Axisymmetric Bending Stresses in Solid Circular Plates with Thermal Gradients, Readers' Forum, J. Aerospace Sci. 27, 717-718 (1960).

9. B. F. Langer, Design Values for Thermal Stress in Ductile Materials, The Welding Journal, Research Supplement 37, 411s-417s (Sept 1958).

10. S. H. Fistedis, Design Criteria for Steel in Nuclear Reactors, ANL-6389 (July 1961).

11. S. H. Fistedis, H. W. Davis, and R. W. Sauer, Steel Design Criteria for Nuclear Applications, Progress Report, J. Structural Division 88, No. ST-1, Proc. Am. Soc. Civil Engrs., pp. 171-186 (Feb 1962).

X

ARGONNE NATIONAL LAB WEST
3 4444 00009014 2